Interannual and Interdecadal Rainfall Variations in the Hawaiian Islands*

PAO-SHIN CHU AND HUAIQUN CHEN

Department of Meteorology, School of Ocean and Earth Science and Technology, University of Hawaii at Manoa, Honolulu, Hawaii

ABSTRACT

Hawaii rainfall has exhibited both interannual and interdecadal variations. On the interannual time scale, Hawaii tends to be dry during most El Niño events, but low rainfall also occurred in the absence of El Niño. On the interdecadal time scale, Hawaii rainfall is negatively and significantly correlated with the Pacific decadal oscillation (PDO) signal; an epoch of low rainfall persists from the mid-1970s to 2001, which is preceded by an epoch of high rainfall lasting for nearly 28 yr.

Difference patterns in winter [November–December–January–February–March (NDJFM)] rainfall are investigated for composites of extremely dry and wet winters during the dry and wet epochs, respectively. These patterns (i.e., DRY minus WET) are then compared to the difference in constructive match conditions of El Niño and PDO (i.e., El Niño/+PDO minus La Niña/−PDO). Relative to the El Niño/PDO stage, the magnitude of dryness during the rainfall-based stage is enhanced. The corresponding large-scale atmospheric circulation composites are studied. Similar patterns are revealed between these two stages. However, anomalously stronger and deeper sinking motions over Hawaii are revealed in the height–latitude section of the rainfall-based analysis compared to the El Niño/PDO stage. Moreover, an anomalous zonal circulation cell is well established over the subtropical North Pacific with a pronounced descending branch over Hawaii in the rainfall-based stage. The band of anomalous surface westerlies to the north of Hawaii, and the deep sinking motion as well as the anomalously vertically integrated moisture flux divergence over Hawaii are all unfavorable for rainfall in Hawaii.

1. Introduction

It is well known that the tropical North Pacific ocean–atmosphere system fluctuates on a time scale of 2–8 yr, which is called the El Niño–Southern Oscillation (ENSO) cycle (e.g., Rasmusson and Carpenter 1982). The ENSO extremes are labeled as either a warm or cold phase yet its amplitude varies across a continuum with essentially Gaussian statistics (Trenberth 1997). Characterizing the warm ENSO (El Niño) phase are the anomalously deep Aleutian low, cold western and central North Pacific, and anomalous warming in the central and eastern tropical Pacific. The reversed circulation pattern characterizes the cold ENSO (La Niña) phase.

In the late twentieth century, the low-frequency variation of the North Pacific system was revealed (e.g., Trenberth and Hurrell 1994; Zhang et al. 1997; Mantua et al. 1997; Minobe and Mantua 1999) and was named the Pacific decadal oscillation (PDO) (Mantua et al. 1997). The PDO extremes are also labeled as either warm (positive) or cold (negative) phase. The spatial patterns associated with the positive (negative) PDO phase are similar to the warm (cold) ENSO phase. However, the PDO climatic signals, unlike those associated with ENSO, persist for 20 yr or longer. Moreover, PDO's climatic signal is more evident in the midlatitudes, in contrast to ENSO's tropical signal.

The similar spatial pattern of ENSO and PDO suggests that the PDO can modulate the ENSO. Recent research, however, demonstrates that the PDO is driven by ENSO, the North Pacific sea surface temperature anomalies, and random atmospheric forcing (Newman et al. 2003). Therefore, the PDO and ENSO are not independent of each other but are inherently related. Previous studies working on joint ENSO–PDO impacts on climate focused primarily on changes in sea

level pressure, precipitation, and surface temperatures over the continental United States (Gershunov and Barnett 1998; Gershunov 1998; Gershunov and Cayan 1999; Bove 2000). Gershunov and coinvestigators found that during constructive match conditions (i.e., El Niño/+PDO and La Niña/−PDO), the corresponding winter ENSO pattern over the U.S. continent is intensified, while the opposite match conditions (e.g., El Niño/−PDO) are destructive to the ENSO pattern. However, the combined effects of ENSO and PDO are not uniform over the United States and are season dependent.

Because of the proximity of the Hawaiian Islands to the centers of ENSO and PDO, it is expected that both the ENSO and PDO cycles influence Hawaiian rainfall. Hawaiian winter rainfall anomalies associated with extremes in the ENSO are widely accepted (Lyons 1982; Taylor 1984; Ropelewski and Halpert 1987; Chu 1989, 1995; Cayan and Peterson 1989). Chu (1995) proposed a mechanism that could result in the deficient rainfall during El Niño winter in Hawaii. During El Niño winter, the upper-tropospheric jet stream extends eastward. Hawaii is located in the right exit region of the jet stream, in an area of upper-level convergence. The expected anomalous sinking motion resulting from the upper-level convergence tends to inhibit both the development and maintenance of subtropical cyclones over Hawaii and the southeastward propagation of strong frontal systems into the island chain.

Hawaii winter rainfall is also found to have a negative correlation with the PDO (Mantua et al. 1997). As will be seen shortly, Hawaii rainfall has exhibited a clear signal for interdecadal variations. No previous work has been done to investigate large-scale atmospheric circulation variations associated with Hawaii's interdecadal patterns. Moreover, given the similar circulation patterns of ENSO and PDO, it remains interesting to determine the joint impact of ENSO/PDO extremes on Hawaiian rainfall anomalies. In section 2, the dataset and data processing are described, followed by the methodology in section 3. The background rainfall climatology is given in section 4. Results from the statistical analysis are discussed in section 5. Section 6 discusses large-scale atmospheric circulation during extreme climatic events. A summary is found in section 7.

2. Data and data processing

a. Data

The National Weather Service cooperative stations provide the monthly precipitation data (TD3220) used in this study. The station data can be obtained from the National Climatic Data Center (NCDC) Web page.
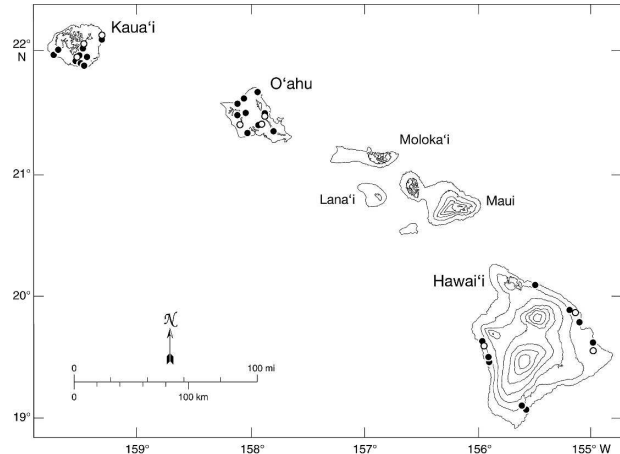

FIG. 1. Map of the major Hawaiian Islands and the location of 27 stations used to construct the HRI. An open circle indicates a new station used to replace the adjacent old station (solid circle). Contour interval for elevation is 2000 ft.

Only the stations with records longer than 20 yr are selected. The data period is from 1950 to 2002. In all, there are 272 stations included.

The circulation data used in this study are the National Centers for Environmental Prediction–National Center for Atmospheric Research (NCEP–NCAR) reanalysis data on a 2.5° latitude × 2.5° longitude grid. The data include monthly mean horizontal winds, specific humidity, and vertical velocity at standard pressure levels. The SST data come from the Reynolds reconstructed dataset, with a resolution of 2° latitude × 2° longitude.

b. Climatic indices

1) HAWAII RAINFALL INDEX

The Hawaii rainfall index (HRI) has been used in several studies (Meisner 1976; Taylor 1984; Chu 1989, 1995). This monthly index, which represents rainfall variations over different climate regions of the Hawaiian Islands, was originally developed by Meisner (1976). The monthly rainfall data from nine stations on each of three islands (Kauai, Oahu, and the Island of Hawaii) were used to construct the HRI, resulting in a total of 27 stations (Fig. 1 and Table 1). The stations represent rainfall from varying elevations (i.e., high, medium, and low) and varying locations with respect to the trade wind direction (i.e., windward, neutral, and leeward). Because some gauges are discontinued, more recent records from adjacent stations are used. These new stations are denoted by an asterisk in Table 1 and an open circle in Fig. 1.

T ABLE 1. Rainfall stations used for HRI. Solidus denotes that replacement station follows. Asterisk denotes new stations.

Island	Station	Code no.	Lat (°N)/Lon (°W)	Elevation (m)	Record length
Kauai	1. Iliilula Intake/North Wailua Ditch*	1050.00	22°02′34″/159°28′18″	326.2	1935–86
		1051.00	22°03′57″/159°28′12″	338.4	1987–2000
	2. Koloa Mauka	994.00	21°57′50″/159°26′36″	195.1	1905–2002
	3. Kealia/Anahola*	1112.00	22°06′10″/159°18′30″	3.0	1905–86
		1114.00	22°08′15″/159°18′24″	54.9	1987–2000
	4. Wahiawa Mt./Alexander Reservoir*	990.00	21°58′30″/159°30′35″	655.4	1905–72
		983.00	21°57′34″/159°31′43″	423.6	1973–2002
	5. East Lawai	934.00	21°54′30″/159°29′48″	134.1	1905–2002
	6. Kukuiula	935.00	21°53′30″/159°29′30″	32.0	1905–2002
	7. Puehu Ridge	1040.00	22°01′07″/159°41′42″	506.1	1940–2000
	8. Brydeswood Station	985.00	21°55′42″/159°32′12″	219.5	1910–2002
	9. Waiawa	943.00	21°58′50″/159°43′58″	3.0	1905–99
Oahu	10. Nuuanu Res.	783.00	21°21′21″/157°48′37″	320.1	1905–2002
	11. Waikane/Waiahola*	885.00	21°30′12″/157°53′24″	243.9	1917–82
		837.00	21°28′24″/157°52′58″	227.1	1983–2002
	12. Kahuku	912.00	21°40′48″/157°57′12″	7.6	1905–2002
	13. Wahiawa Dam	863.00	21°30′00″/158°03′08″	260.6	1905–99
	14. Waimea	892.00	21°37′43″/158°04′03″	128.0	1917–2002
	15. Waialua	847.00	21°34′36″/158°07′24″	4.5	1905–2000
	16. Waianae Mauka/Hokuloa*	803.00	21°29′25″/158°08′04″	480.1	1905–73
		725.20	21°24′36″/158°05′48″	594.7	1974–99
	17. Aiea Field/Aiea*	761.00	21°24′30″/157°56′36″	138.7	1908–69
		764.50	21°24′26″/157°54′35″	213.4	1970–2002
	18. Ewa Mill	741.00	21°20′38″/158°02′12″	22.8	1905–2002
Hawaii	19. Hakalau Mauka/Honomu Mauka*	135.00	19°53′12″/155°10′06″	350.6	1906–78
		138.00	19°51′06″/155°08′48″	382.8	1979–2002
	20. Paauhau	217.00	20°05′12″/155°26′24″	121.9	1905–99
	21. Papaiku Makai	144.10	19°47′12″/155°26′24″	60.9	1905–2002
	22. Kiolakaa	6.00	19°04′24″/155°38′18″	586.8	1929–98
	23. Naalehu	14.00	19°03′48″/155°38′18″	205.7	1905–2002
	24. Kapolo/Hayhalalekai*	93.00	19°30′48″/155°35′24″	33.5	1905–59
		67.50	19°28′30″/154°50′06″	4.6	1960–2002
	25. Kaawaloa	29.00	19°29′42″/155°55′12″	408.5	1942–99
	26. Napoopoo	28.00	19°28′18″/155°58′30″	121.9	1940–2002
	27. Halualoa Beach/Kainaliu Beach*	68.00	19°36′30″/155°58′47″	53.0	1919–78
		73.12	19°31′54″/155°57′24″	5.2	1979–98

2) PDO INDEX

The PDO index (PDOI) defined by Mantua et al. (1997) is used in this study to characterize the Pacific low-frequency variability (available online at http://tao.atmos.washington.edu/pdo/). The PDOI is defined as the leading principal component of the monthly North Pacific (poleward of 20°N) SST anomaly residuals, whereas residuals are understood as the gridpoint anomalies after the global mean monthly SST anomaly is removed from every location (Zhang et al. 1997). Positive values of this index describe anomalously cold SST anomalies around 45°N. Several studies found evidence for PDO cycles during the past century (e.g., Trenberth and Hurrell 1994; Minobe 1997; Zhang et al. 1997; Mantua et al. 1997). The negative PDO phase prevailed from 1947 to 1976 while the positive PDO phase dominated from 1925 to 1946 and from 1977 to

1999 (see online at http://sealevel.jpl.nasa.gov/science/pdo.html).

3) NORTH PACIFIC INDEX

The North Pacific index (NPI; Trenberth and Hurrell 1994) measures the strength of the Aleutian low during the boreal cool season. The NPI is defined as the area-weighted mean sea level pressure over the region 30°–65°N, 160°E–140°W (data available online at http://www.cgd.ucar.edu/cas/jhurrell/indices.html).

4) ENSO INDEX

Niño-3.4 was chosen as the ENSO index because it is more representative of ENSO than other indices (e.g., Barnston et al. 1997). Here, we used Trenberth's (1997) definition of Niño-3.4 index (available online at http://www.cgd.ucar.edu/cas/catalog/climind/TNI_N34/index.

html); according to his definition, El Niño (La Niña) occurs if a 5-month running mean of SST anomalies in the Niño-3.4 region (5°N–5°S, 120°–170°W) exceeds 0.4°C (-0.4°C) for six consecutive months or more.

3. Methodology

a. Eleven-year or five-month running mean

To detect the low-frequency variability of Hawaiian rainfall, an 11-yr running mean is applied to the annual HRI time series. Because the peak rainy season in Hawaii occurs in winter, and to keep this season intact, we use the water year calendar from July to June of the following year in accordance with the November–March rainy season. The annual rainfall is obtained by summing the monthly precipitation values for each station. As an example, the sum of the monthly rainfall from July 1995 to June 1996 is taken as the annual rainfall of 1996.

An 11-yr running mean is then applied to the standardized annual rainfall (SAR) time series to remove the high-frequency interannual variations (e.g., Garbrecht and Rossel 2002). The SAR is calculated by taking the difference between the individual annual rainfall value and the long-term mean annual value, and then dividing this difference by the standard deviation of the annual rainfall amount. The filtered data, $X_\ell(t)$, are expressed as

$$X_\ell(t) = \frac{1}{11} \sum_{j=-5}^{5} X(t + j), \qquad (1)$$

where the subscript $_\ell$ denotes a low-pass filtering and X represents SAP. The operation in (1) clearly precludes the use of the first and last five points in the records. It is also desirable to obtain filtered values for these end points. To obtain them, for example, the first filtered value is taken as the average of the first six unfiltered SAR, the second filtered value is the average of the first seven unfiltered SAR, and so on. For detecting the interannual variation of Hawaiian rainfall and its relationship to the Niño-3.4 index, a similar procedure is used to calculate the 5-month running mean of Hawaii rainfall.

b. Wavelet analysis

Wavelet analysis is a powerful tool for analyzing the temporal frequency change. Using wavelet analysis, one can determine both the dominant modes of variability and how these modes vary in time. In this study, the Morlet wavelet analysis is employed to detect the Hawaiian rainfall variations with time. Various applications of wavelet analysis on climate research can be found in Weng and Lau (1994), Lau and Weng (1995), and Torrence and Compo (1998, hereafter TC98).

c. Nonparametric Mann–Whitney test

A nonparametric Mann–Whitney rank-sum test is used to evaluate the rainfall difference in location between two independent data samples (Wilks 1995). The null hypothesis is that the two datasets have the same location (i.e., overall magnitude). Assume that we have two batches of sample data, with sample sizes n_1 and n_2 ($n = n_1 + n_2$), respectively. To perform this test, the two data batches need to be pooled and ranked. Let U be the Mann–Whitney statistic

$$\begin{aligned} U_1 &= R_1 - \frac{n_1}{2}(n_1 + 1) \\ U_2 &= R_2 - \frac{n_2}{2}(n_2 + 1) \end{aligned}, \qquad (2)$$

where R_1 and R_2 are defined as the sum of the ranks held by the batches 1 and 2, respectively. The null distribution of the Mann–Whitney U statistic is approximately Gaussian when n_1 or n_2 is moderately large with

$$\mu_U = \frac{n_1 n_2}{2} \qquad (3)$$

$$\sigma_U = \left[\frac{n_1 n_2 (n_1 + n_2 + 1)}{12} \right]^{1/2}. \qquad (4)$$

Once μ_U, σ_U, and U_1 (or U_2) are computed, the U statistic at each grid point is transformed into a standard Gaussian variable and is evaluated for its statistical significance (Chu 2002).

d. Moisture field

Water vapor is an important ingredient for convection. In general, moisture divergence patterns correspond well with rainfall anomaly composites. The vertically integrated water vapor flux can be computed from the horizontal moisture flux given by (Newell et al. 1974)

$$\mathbf{Q} = \frac{1}{g} \int_{p_1}^{p_2} q\mathbf{V} \, dp, \qquad (5)$$

where q is specific humidity (g kg^{-1}) and $\mathbf{V}$ is the horizontal wind vector in meters per second. The vertical integration in (5) is performed for eight standard atmospheric levels from 1000 to 300 mb. The divergence of the vertically integrated water vapor flux is calculated by taking the divergence of Eq. (5) as

$$\boldsymbol{\nabla} \cdot \mathbf{Q} = \frac{1}{g} \int_{p_1}^{p_2} \boldsymbol{\nabla} \cdot (q\mathbf{V}) \, dp. \qquad (6)$$

4. An overview of annual rainfall cycle in Hawaii

The annual cycle of rainfall in Hawaii is characterized by two seasons: summer and winter. Summer extends from May to October and is a dry season with northeasterly trade winds from the sea. Cumulus clouds associated with the quasi-permanent subtropical high in the eastern North Pacific are constantly advected toward the islands. Regions of maximum rainfall are usually located on windward slopes where orographic uplifting is most pronounced. On the leeward side of the mountains, air sinks and warms, suppressing the development of rain showers there. This is known as the rain shadow phenomenon. High mountain tops well above 3000 m even on the eastern slopes are also dry because low-level moisture-laden trade winds are capped by the subsidence inversion, which usually occurs at a height of about 2000 m (Chen and Feng 1995).

For the winter rainy season, which generally extends from November to March, trades are often interrupted by midlatitude frontal systems, Kona storms, and upper-level troughs or lows (e.g., Ramage 1962; Blumenstock and Price 1967; Chu et al. 1993; Morrison and Businger 2001). Cold front passages may bring light to moderate rainfall to the Hawaiian Islands. Because of the modification of cold air by the underlying warm seawater, cold fronts approaching the islands from the northwest usually lose their distinct temperature contrasts across the front and manifest themselves as wind shear lines. Kona storms are cutoff lows in the upper-level subtropical westerlies. They usually occur to the north of Hawaii, and many are associated with surface lows. Kona storms last for days or even a week and occasionally bring torrential rain to the islands. In general, Kona rains are more widespread and more abundant than the cold front–induced rainfall. The presence of an upper-level trough or low to the northwest of the islands helps produce unstable conditions with heavy rainfall. Upper-level lows usually are not persistent and sometimes are not marked by strong, low-level southerly winds that generally accompany Kona storms. Note that although the aforementioned three types of weather disturbances are major producers of winter rainfall, trade wind is still an important source of rainfall even in the cool season (Lyons 1982).

5. Statistical analysis

a. Interannual variability

The results shown in Fig. 2 are the 5-month running mean of the Niño-3.4 index and HRI for the period July 1905–June 2001. An out-of-phase relation between the interannual variation of the Hawaiian rainfall and that
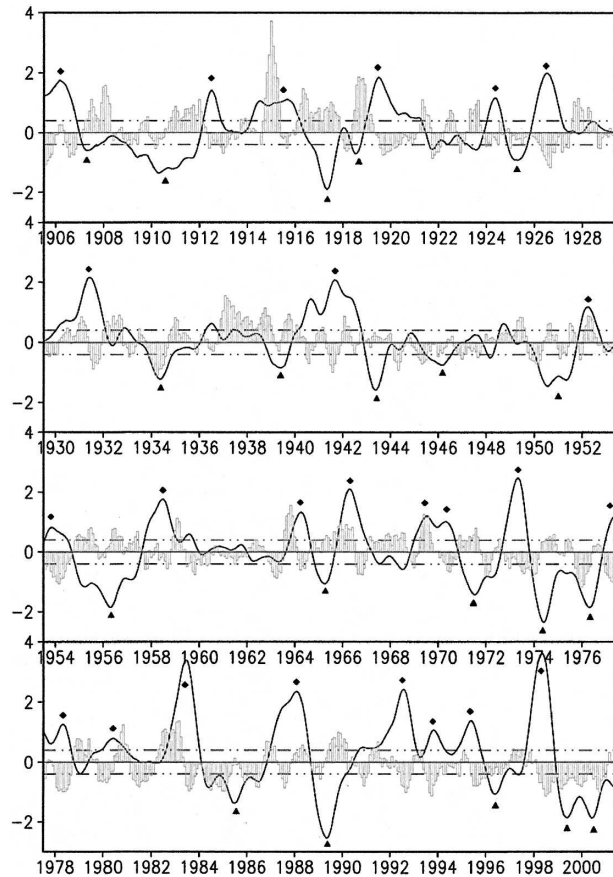

FIG. 2. Time series of 5-month running mean of Niño-3.4 index (line) and HRI (bar), and the dashed lines are ±0.4°C as the definition of Niño-3.4. Diamonds indicate El Niño events and triangles indicate La Niña events.

of the Niño-3.4 SST anomaly for most of the entire period can be identified, which was originally proposed by Walker and Bliss (1932). For most of the El Niño events (indicated by diamonds) rainfall over Hawaii tends to be below normal while for most of the La Niña events (indicated by triangles) Hawaiian rainfall is above normal. However, some of the El Niño events are marked by abundant rainfall in Hawaii, such as the 1969 El Niño event, and extremely dry winters in Hawaii occurred in some La Niña years, such as the 1999–2000 La Niña event.

b. Interdecadal variability

To depict the low-frequency rainfall variability, an 11-yr running mean is applied to the normalized annual precipitation time series, as well as the normalized PDOI (Fig. 3a). Interdecadal variations of the HRI and PDOI are easily recognized. The negative relationship between the HRI and the PDOI on decadal time scales
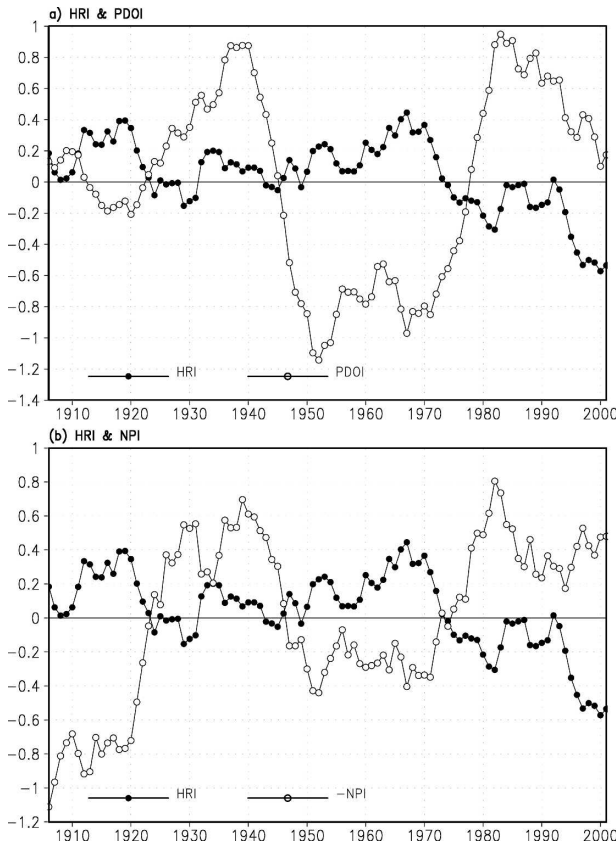
FIG. 3. (a) Time series of 11-yr running mean (based on the water year from Jul to Jun of the following year) for HRI (closed circle) and PDOI (open circle). (b) Same as (a) except for reversed NPI (−NPI, open circle).

is also evident in Fig. 3, and is consistent with the result of Mantua et al. (1997). The Hawaii rainfall had two above-normal epochs (i.e., wet periods) on the decadal time scales: one from 1906 to 1923 and the other from 1946 to 1973. A recent epoch with a negative rainfall anomaly persisted from 1974 to 2001. The PDOI also had two below-normal epochs, during 1913–1922 and 1946–1977. The positive PDO regimes prevailed from 1923 to 1945 and from 1978 to 2001. Note that the positive PDOI values from 1906 to 1912 are not consistent with the PDO cycles of Mantua et al. (1997). This is probably due to the application of an incomplete 11-yr running mean at each end of the time series in Fig. 3a. For the same reason, a turnabout of the PDO from positive to negative phase starting from around 1999 (see online at http://sealevel.jpl.nasa.gov/science/pdo.html) is not evident in Fig. 3a. Broadly speaking, the HRI seems to vary, in a negative sense, the decadal oscillation of the PDOI, except for two early periods (1906–12 and 1924–45) when an out-of-phase relationship between these two indices seems to break down.

The major transitions in the decadal Hawaii rainfall correspond approximately with similar transitions in the decadal signal of PDOI. The slight shift of PDOI transition points compared to a previous study by Mantua et al. (1997) is due to the difference in applying the running mean and the definition of the water year in this study. Figure 3b displays the time series of the HRI and the NPI. For easy comparison, the sign of NPI is reversed. The positive relationship between HRI and the original NPI series can be identified. The relationship between HRI and NPI also breaks down during 1924–46.

c. Wavelet analysis of rainfall series

Figure 4a displays the time series of the winter (NDJFM) rainfall anomaly in Hawaii. The extended seasonal values are used in the wavelet analysis because they provide a better isolation of multidecadal effects than those based on the monthly data. In Fig. 4a, a clear downward trend in rainfall is noted. In particular, there is a relatively high frequency of low rainfall years since approximately 1970.

The power spectrum of the rainfall records is shown in Fig. 4b, giving the information of the change in energy density with time. It reveals that energy is concentrated on the interannual (2–6 yr) and interdecadal (approximately between 12 and 20 yr) time scales. From 1910s to the mid-1970s, the HRI was dominated by the interdecadal variability while the quasi-5.7-yr cycle waxed and waned during this period. Since the late 1970s, the interdecadal signal becomes weaker and the dominant oscillations appear to be somewhere around 2–3 and 8 yr until the early 1990s.

The real part of the wavelet transform is shown in Fig. 4c, depicting both the intensity and phase of the signal variation at particular scales and locations in wavelet domain. As only the positive values are illustrated, the interdecadal (12–20 yr) signal is well recognized almost throughout the entire record period. As previously mentioned, the filtered annual precipitation series experienced alternations of relatively dry and wet epochs throughout the time (Fig. 3). For instance, the two positive real part signals in the multidecadal time scale (>30 yr) during the 1910s–1920s and 1950s–mid-1970s in Fig. 4c correspond to positive rainfall anomalies (wet epochs) in Fig. 3. However, this signal in Fig. 4c is much weaker and located in the region of the cone of influence (TC98).

d. Quantitative analysis of rainfall variations with ENSO or PDO

To quantify the relationship between Hawaii rainfall and climate extremes, Table 2 lists different ENSO/
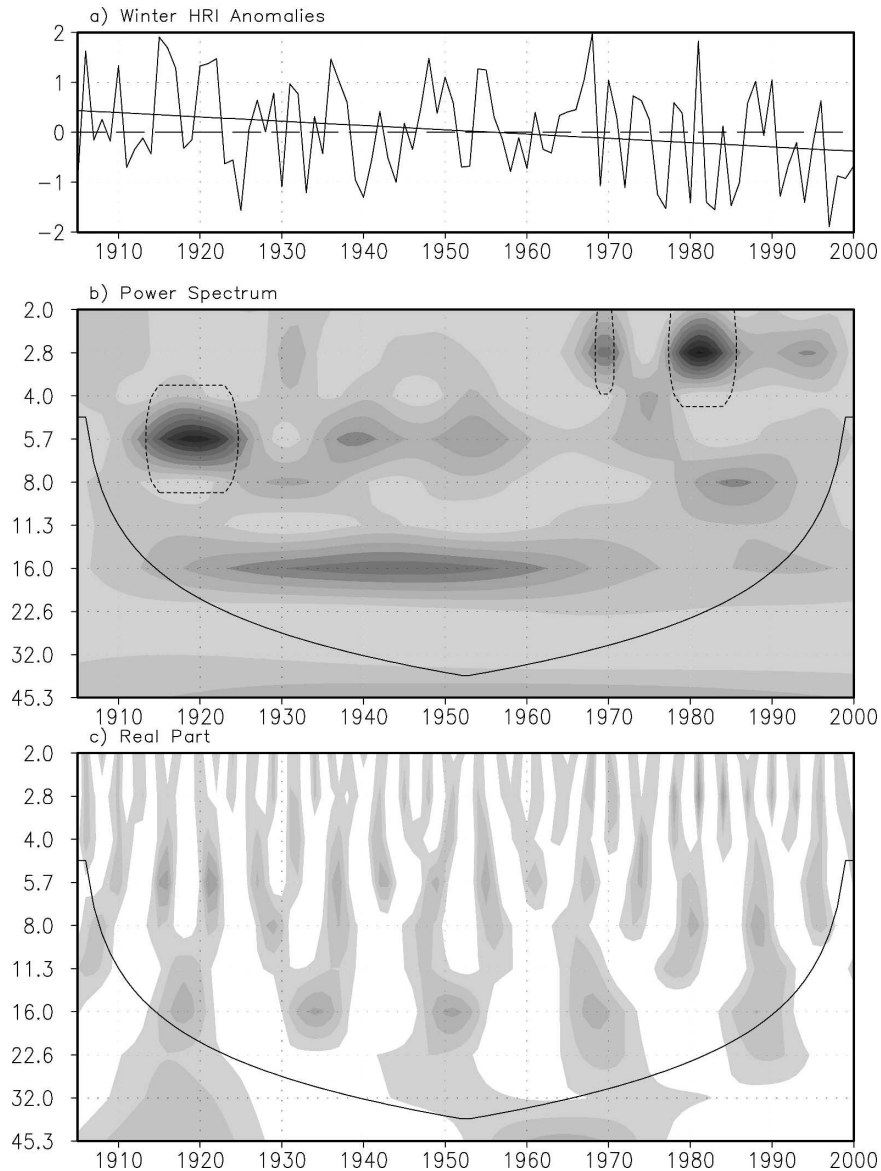
FIG. 4. (a) Time series of winter (NDJFM) HRI anomalies. Straight line denotes the linear regression line fitted to the records. (b) Power spectrum of wavelet analysis, shadings represent different energy density with high amplitude in dark shading and and low amplitude in light shading. Region from curve to the bottom indicates the cone of influence. Broken lines enclose regions of greater than 95% confidence relative to a red-noise process with a lag-1 coefficient of 0.0965; N (sample size) = 96, δt (time interval) = 1, δj (factor for scale averaging) = 0.5, and J = 10, giving a total of 11 scales ranging from 2 to 64 yr. (c) The real part of the wavelet analysis and the shading range are same as (b), except that only the positive values are shown. The Y coordinate in (b) and (c) is scaled in years.

PDO bins since 1951, considering the availability of TD3220 dataset. Years selected from this table provide a basis for the following monthly composites. As an example, the data used for the 1983 warm ENSO run from July 1982 through June 1983. Figure 5a displays the month-to-month composites of the HRI during warm and cold phases of ENSO. Small and positive

rainfall anomalies are noted from July to October during the year when warm ENSO has occurred. Deficient rainfall then persists for six consecutive months from November to April of the following year, with a large negative anomaly in January and February. This is consistent with Chu (1995) who, on the basis of seasonal rainfall records, noted that El Niño–related drought in

TABLE 2. Listings of El Niño (EN), and La Niña (LN) events since 1951. The mean rainfall in inches for winter (NDJFM) for each subset is indicated at the last column; the bold number indicates the highest mean winter rainfall of all, while the underlined number is the lowest mean winter rainfall.

PDO phase	Status	Years	Actual years	Mean
−PDO (1951–76)	EN	5	1952, 1966, 1969, 1970, 1973	37.58
	LN	7	1951, 1955, 1956, 1971, 1974, 1975, 1976	**45.92**
+PDO (1977–99)	EN	7	1977, 1980, 1983, 1987, 1992, 1995, 1998	<u>24.93</u>
	LN	4	1985, 1989, 1996, 1999	36.96

Hawaii is persistent, lasting for about two seasons during winter and spring. Rainfall variations during La Niña events are opposite to that of El Niño and the largest positive anomaly also occurs in January and February. When the difference in rainfall between the warm and cold ENSO composites is considered, the 95% confidence level is reached for the months of October, November, January, and February.

Low rainfall tends to occur from October to May when the PDO is in the positive phase (Fig. 5b). The opposite can be said for the negative PDO phase. However, the magnitude of rainfall anomalies during the PDO composite is smaller than that during the ENSO composite. Only January and February exhibit statistical significance in Fig. 5b. During the synergetic conditions of ENSO and PDO, the patterns appear like the corresponding ENSO-only composites but the magnitude of rainfall anomalies is enhanced (Figs. 5a,c). Again, the large anomalies occur during the extended winter season (NDJFM) with the difference between two climatic stages being significant from November through February (Fig. 5c).

To further give a measure of association between rainfall and low-frequency climate forcings, the Pearson correlations among different running mean indices are calculated and given in Table 3. All correlation coefficients are significant at the 95% confidence level, when Quenouille's (1952) method was used to account for the reduction of effective numbers of degree of freedom due to persistence (Clark and Chu 2002). The higher correlation exists between HRI and NPI, suggesting the important influence of the interdecadal variability in the atmospheric circulation over the North Pacific, as measured by the Aleutian low, on Hawaii rainfall.

e. Rainfall pattern analysis

Results from the previous section reveal that both ENSO and PDO modulate Hawaii winter rainfall. Based on these results, it is instructive to investigate the joint effect of these two climate forcings on Hawaii winter rainfall. Accordingly, rainfall patterns are ana-

lyzed for composites of the El Niño/+PDO and La Niña/−PDO. To compare the rainfall-based composite with the ENSO/PDO-based patterns, a separate but parallel analysis is performed according to in-phase categories of the winter rainfall at the interannual and interdecadal time scales.

Since the TD3220 dataset begins in 1950, the wet epoch runs from 1950 to 1974 and the dry epoch is from 1975 to 2001. Because the winter season is used here, the starting year of the dry epoch is slightly off from that described in section 5b where the annual rainfall index was employed. During the dry epoch, seven dry winters (1978, 1981, 1984, 1986, 1993, 1999, and 2000) with relatively large negative rainfall anomalies are chosen. Note that none of these winters are labeled as El Niño years in Table 2. Similarly, seven wet winters (1952, 1962, 1965, 1966, 1967, 1968, and 1969) with large positive anomalies are selected during the wet epoch. Again, these seven wet winters do not coincide with La Niña events. The two stages considered for comparison include 1) the (dry winters/dry epoch) minus (wet winters/wet epoch) composite, and 2) the (El Niño/+PDO) minus (La Niña/−PDO) composite. For simplicity, the former stage is referred to as DRY minus WET. For each scenario, the nonparametric Mann–Whitney test is applied to evaluate the confidence level of the rainfall difference. The minimum sample size for the test was set to be five for each data batch. Because of the incomplete rainfall records, some stations failed to meet this criterion. As a result, the number of stations used for the significance test is less than that for the corresponding rainfall analysis.

Figure 6a displays the winter rainfall difference pattern between DRY and WET composites for all 272 stations in Hawaii. Almost the entire island chain shows signs of reduced rainfall when the WET composite is subtracted from the DRY. The corresponding nonparametric Mann–Whitney test shown in Fig. 7a provides supporting evidence that this difference is indeed statistically significant. All stations on the islands of Kauai, Oahu, Molokai, and Lanai show confidence at the 90% level with many stations even reaching the 99% level.
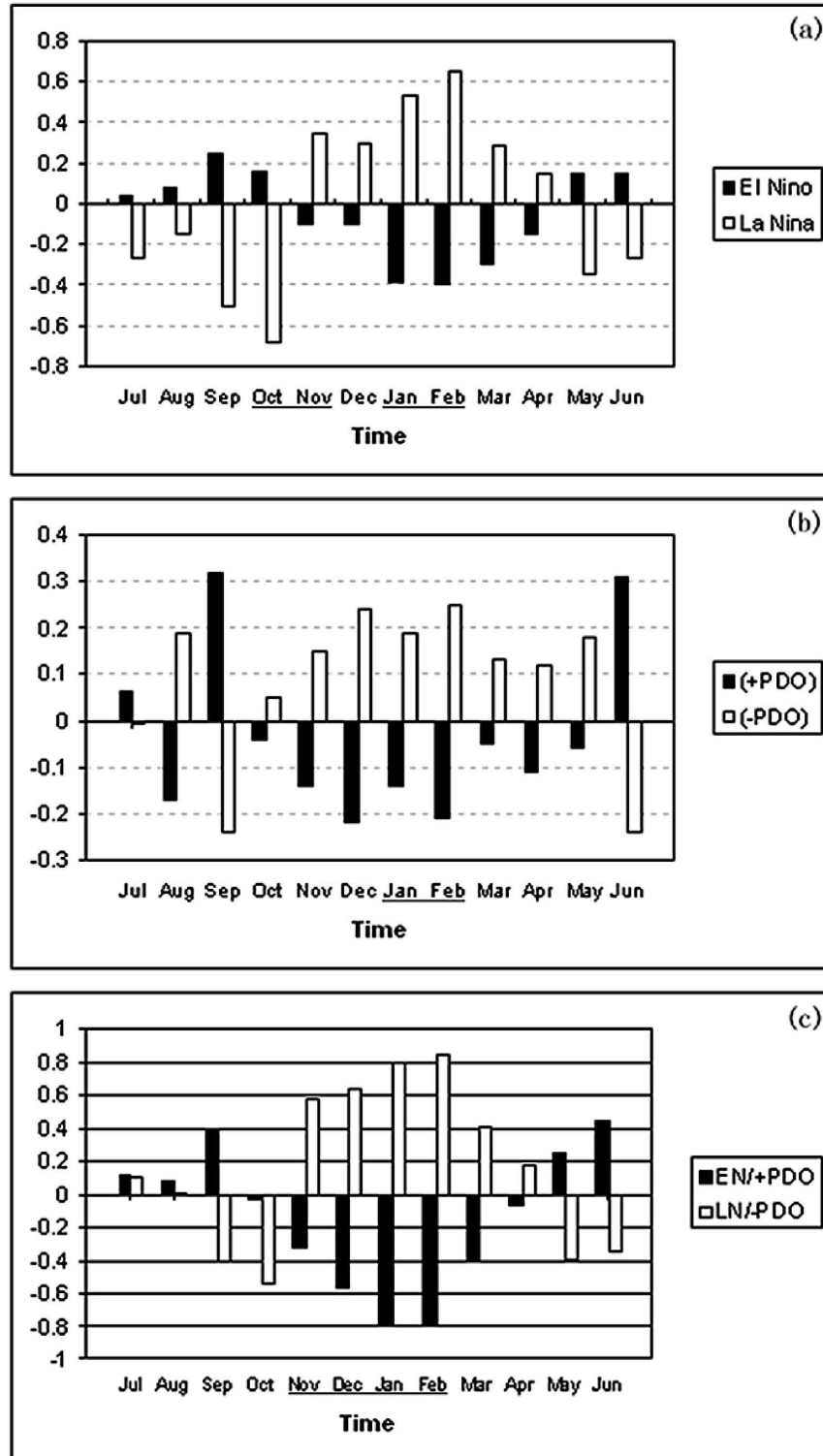
FIG. 5. Time series of composite monthly rainfall index from Jul to Jun during an extreme climatic stage. Normalized HRI value is used. (a) El Niño (filled bar) and La Niña (open bar), (b) Positive PDO (filled bar) and negative PDO (open bar), and (c) El Niño/+PDO (filled bar) and La Niña/−PDO (open bar). Months with underline indicate confidence at the 95% level based on the nonparametric Mann–Whitney test. Note that the vertical scale in each panel is different.

TABLE 3. Pearson correlation coefficients between various 11-yr running mean indices for the period 1906–2001.

	HRI	PDOI	NPI
HRI	1.0		
PDOI	−0.485	1.0	
NPI	0.652	−0.608	1.0

For the two easternmost islands (Maui and Hawaii), the stations that fail to pass the significance test are mostly located in central and windward side of the island. It should be noted that the spline interpolation scheme in the Geographic Information System has been used to fill in the areas between station locations. Therefore, caution must be exercised in areas without extensive data such as the interior of the Island of Hawaii where high mountains loom.

For the El Niño/+PDO and La Niña/−PDO composite (Fig. 6b), dry conditions again prevail. However, relative to the DRY minus WET composite (Fig. 6a), the magnitude of the dry anomalies in Fig. 6b is generally smaller. For the ENSO/PDO composite (Fig. 7b), there are fewer stations on the islands of Hawaii and Lanai showing statistical significance as compared to Fig. 7a. We have also evaluated the rainfall difference composites for the El Niño minus La Niña and the positive PDO minus negative PDO composites separately. In general, the ENSO-only pattern is similar to the joint ENSO/PDO composite exhibited in Fig. 6b, but its signal is weaker than the joint pattern (not shown). The PDO-only pattern also reflects the same effect on Hawaii winter rainfall, though the drying effect is much weaker compared to the ENSO's effect (not shown). Table 2 also lists the winter rainfall mean of each ENSO/PDO subset. Clearly, the El Niño/+PDO is the driest winter subset, while La Niño/−PDO is the wettest winter subset.

6. Large-scale atmospheric circulation during extreme climate events

To help better understand physical mechanisms instrumental for both interannual and interdecadal climate variations in Hawaii, the atmospheric circulation patterns for the El Niño/+PDO minus La Niña/−PDO stage and the decadal scale DRY minus WET stage inferred from the Hawaiian winter rainfall will be presented in the following.

The composite maps of surface wind anomalies and sea surface temperature (SST) anomalies for the aforementioned two extreme climate stages are shown in Fig. 8. For the DRY minus WET winters (Fig. 8a), anomalously cyclonic circulation is observed over mid-

latitudes with a band of enhanced surface westerly anomalies and cold SSTs to the north of Hawaii. Anomalous midlatitude westerlies may enhance evaporation and ocean mixing west and south of the cyclone, resulting in cooling of ocean surface observed in the western and central North Pacific. Anomalously warm waters associated with southerlies prevail in the extreme eastern North Pacific. Southerly anomalies on the eastern flank of the cyclone may increase onshore Ekman transport, with the effect of suppressing coastal upwelling. This effect, together with warm water directly being advected by southerly anomalies, results in anomalous warming along the west coast of North America.

For the ENSO/PDO subset (Fig. 8b), the anomalous surface wind circulation over the North Pacific remains essentially the same as the DRY minus WET composite (Fig. 8a), indicating a deepening of the Aleutian low. However, as expected, positive SST anomalies prevail in the equatorial eastern and central Pacific in Fig. 8b and the warming in the eastern Pacific in the ENSO/PDO composite seem to be enhanced relative to that in Fig. 8a. The cool pool over the central North Pacific in the ENSO/PDO map seems to shift equatorward relative to that in Fig. 8a. Variations of local SSTs in the vicinity of Hawaii are small from Figs. 8a to 8b but nevertheless in an opposite phase. For both stages (Figs. 8a,b), strong surface westerly anomalies prevail over Hawaii, which weaken the climatological easterly trade winds over the subtropical North Pacific. The weakening of trade winds implies a reduction in trade wind rainfall, contributing to dry conditions over Hawaii.

The subtropical jet stream at 200 hPa is examined at each climate extreme. Figure 9 represents the 200-mb composite winter wind field. The jet core is defined as a region where wind speed exceeds 40 m s^{-1} (Chu 1995). The leading edge of the jet core shows a pronounced eastward displacement during the DRY winter than during the WET phase (Figs. 9a,b). This is seen as the jet core elongates well eastward to about 160°W during the DRY phase. In comparison, the jet core retreats westward to around the date line during the WET winter. The zonal displacement of the jet core is also dramatic during the ENSO/PDO stage (Figs. 9c,d). In both Figs. 9a and 9c, Hawaii is located near the right exit region of the jet core in an area of upper-level convergence, which is conducive to midtropospheric subsidence and lower-tropospheric divergence.

From the above upper-level circulation patterns, persistent sinking motion is inferred over Hawaii during DRY winters or warm ENSO when the PDO is in the positive phase. To quantitatively establish this relation,
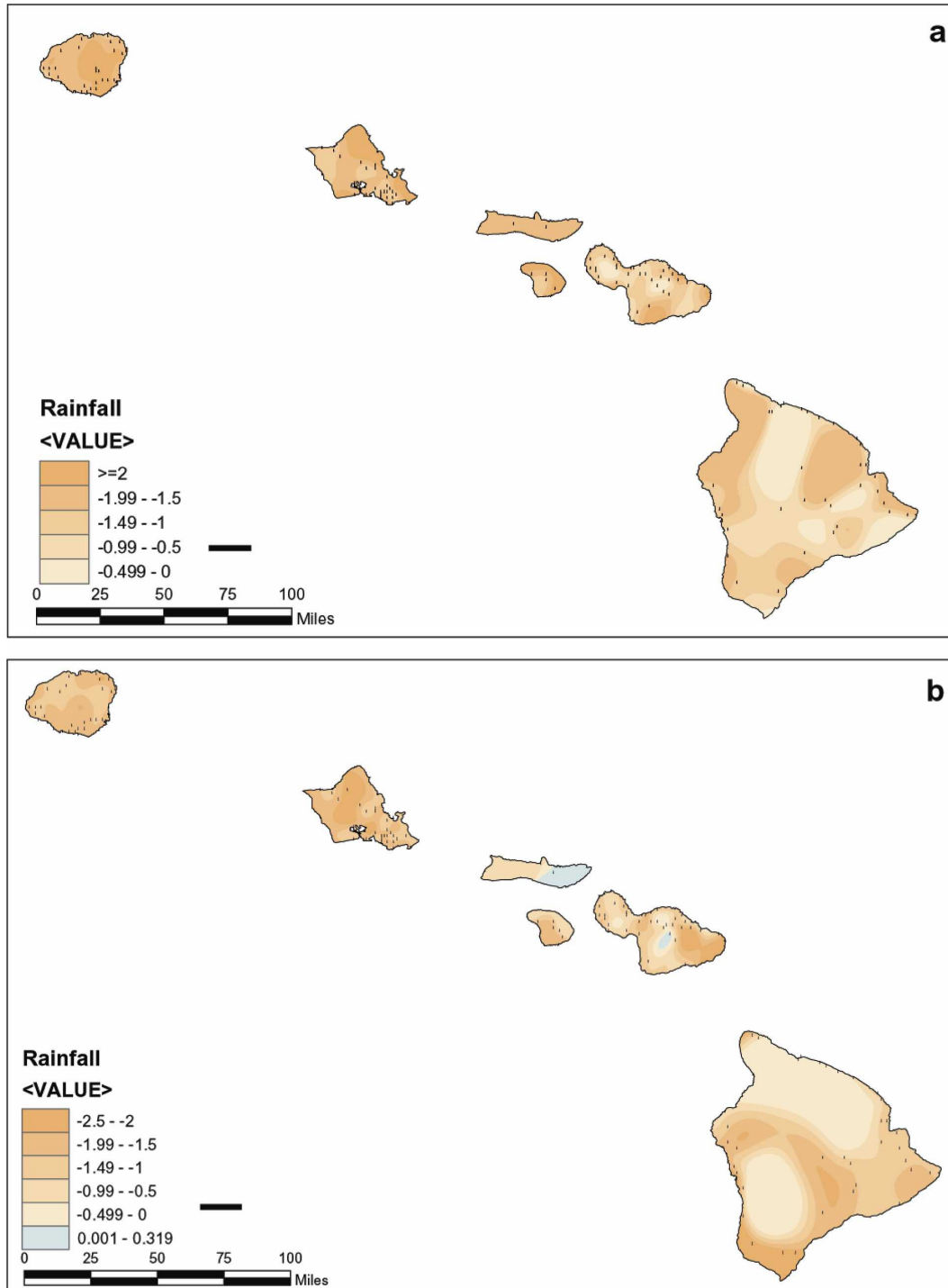
FIG. 6. Winter (NDJFM) rainfall difference (in inches) of the (a) DRY minus WET and (b) (El Niño/+PDO)
minus (La Niña/−PDO) composites. Dots denote rainfall stations.

the vertical cross-section-composites are presented. The north–south vertical cross-section a composite is obtained by averaging the meridional wind component and the negative pressure vertical velocity between

150° and 165°W at 11 standard pressure levels from 1000 to 100 hPa. The height–latitude section depicts the vertical meridional circulation difference between the climate extremes. In Fig. 10a, a broad region of sinking
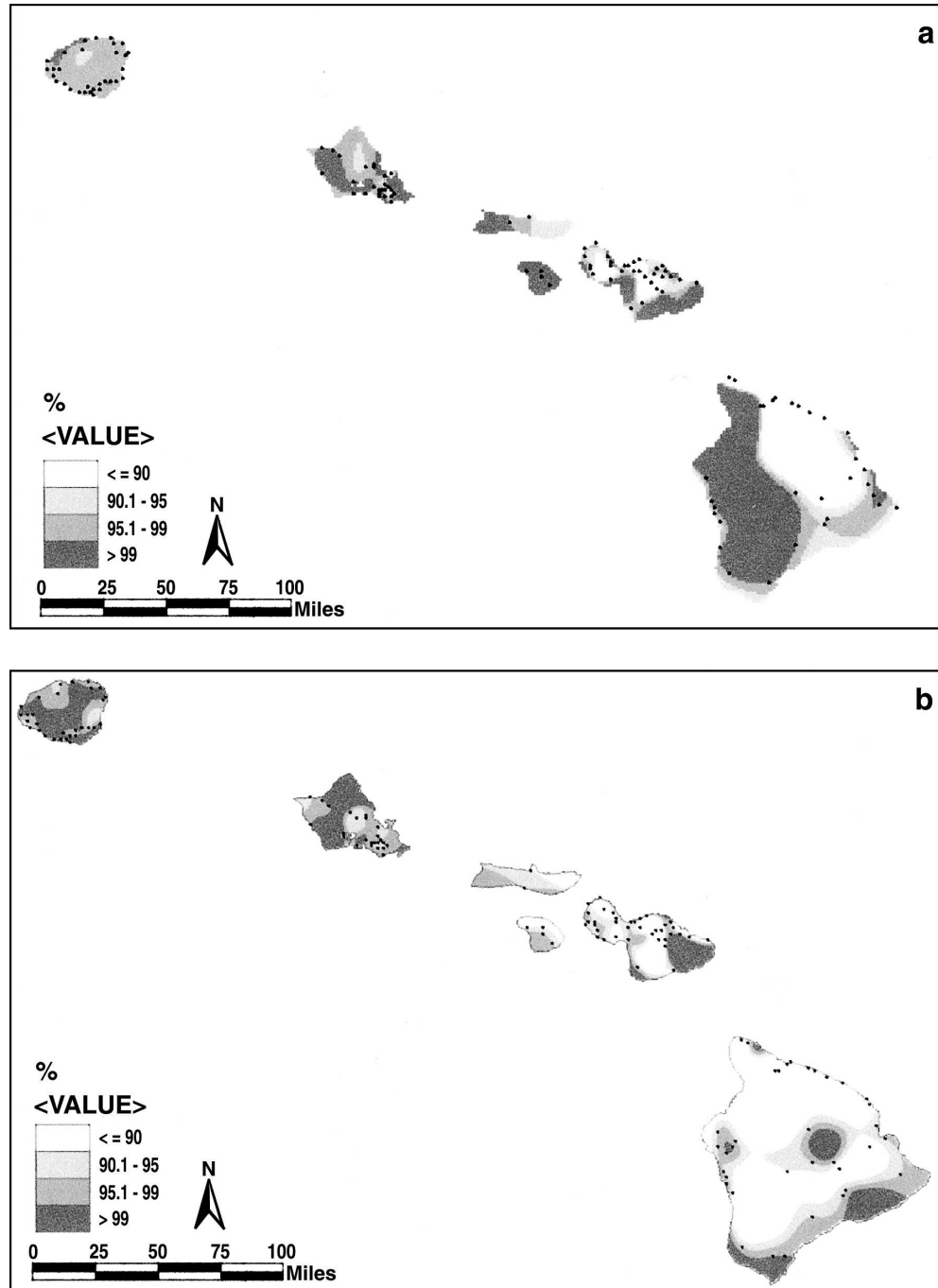
FIG. 7. The nonparametric Mann–Whitney test for winter rainfall difference of the (a) DRY minus WET, and (b) (El Niño/+PDO) minus (La Niña/−PDO) composites. Dots denote stations for testing.

motion is found between 5°S and 25°N extending to almost the entire troposphere. However, the major subsidence branches occur near the latitudes of Hawaii and near the equator, as supported by statistical testing. For the ENSO/PDO composite (Fig. 10b), the North Pacific is dominated by anomalous descending motions from 5° to 30°N but the sinking branch over Hawaii is not as pronounced as the rainfall-based analysis (Fig. 10a).
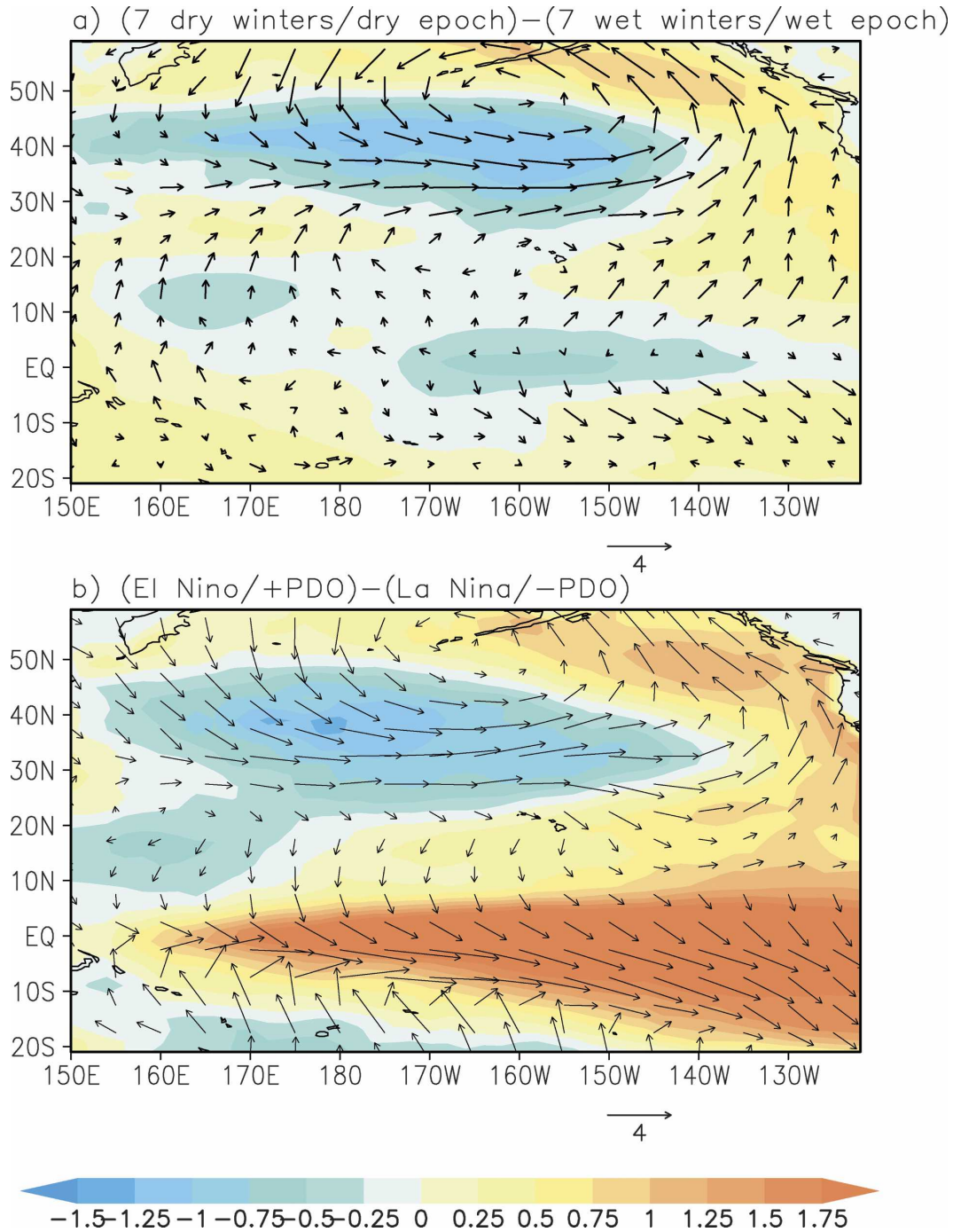
FIG. 8. Winter composites of SST (shading) and surface wind (vectors): (a) DRY minus WET and (b) (El Niño/+PDO) minus (La Niña/−PDO). The unit for SST is °C, and unit for wind vectors is m s^{-1}.

The structure of the east–west vertical cross section is also investigated. It is obtained by averaging the zonal wind component and negative pressure vertical velocity between 15° and 25°N at 11 standard pressure levels from 1000 to 100 hPa. The most salient feature in Fig. 11a is the presence of an anomalous, regional zonal circulation cell over the subtropical North Pacific with an ascending branch near 140°E and a descending branch over 160°W. Hawaii is located right in the region of sinking motions. Also note that the anomalous vertical motions in the aforementioned two branches of the zonal cell not only extend deep to the upper tropo-
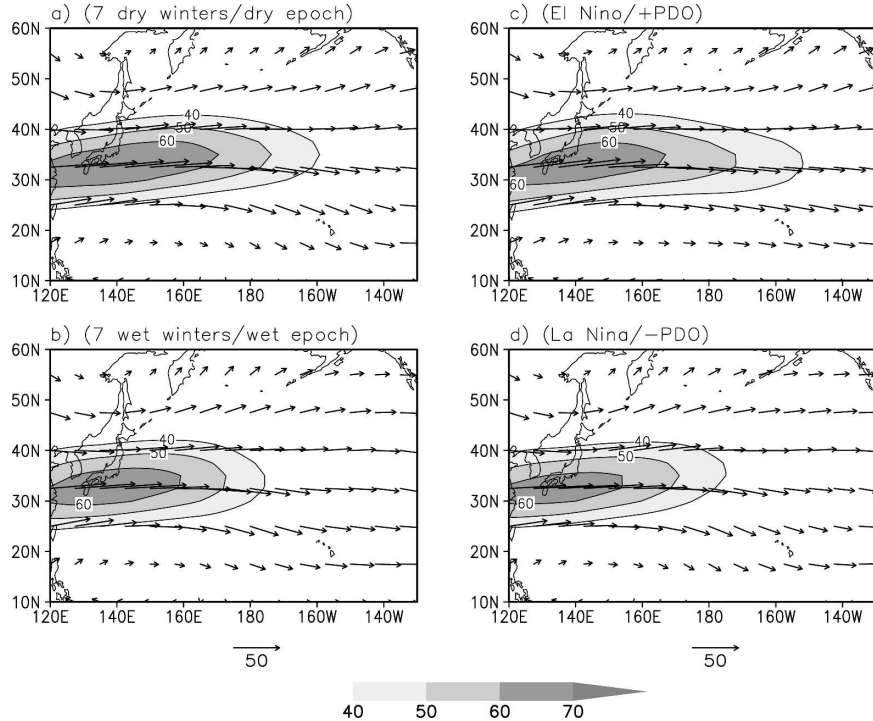
FIG. 9. Winter 200-mb wind (vectors): (a) DRY, (b) WET, (c) El Niño/+PDO, and (d) La Niña/−PDO. Isotach interval is 10 m s^{-1}. Area with wind speed greater than 40 m s^{-1} is shaded.

sphere but also are statistically significant. For the ENSO/PDO winters (Fig. 11b), the cross section is characterized by two large-scale zonal circulation cells: anomalous rising motions in the eastern (100°W) and the western Pacific (120°E), and a broad anomalous sinking motion between 150°E and 150°W, stretching approximately a longitudinal span of 60°. In contrast to the ENSO/PDO winters, the sinking branch revealed in the DRY minus WET composite (Fig. 11a) is more narrowly concentrated between 170° and 150°W and the regional zonal circulation is well recognized. Combining Figs. 10a and 11a, the east–west and north–south vertical circulations have common and pronounced anomalous descending motion over the central subtropical North Pacific concurrent to dry winters in Hawaii. Sinking motion anomalies result in low-level divergence over Hawaii and suppress convection.

An additional insight into the relationship between Hawaii winter rainfall and large-scale circulation can be gained by examining changes in vertically integrated moisture flux and its divergence. The composite differences of the water vapor flux and its divergence for the two extreme stages are given in Fig. 12. For the rainfall-based analysis (Fig. 12a), the moisture flux pattern indicates an anomalous cyclonic circulation over the midlatitude North Pacific with anomalous moisture flux

convergence over the anomalously warm eastern North Pacific (Fig. 8a). Moisture flux divergence anomalies over the Hawaiian Islands and a band of flux convergence anomalies over the subtropical western North Pacific are consistent with the regional zonal circulation cell whose sinking branch is over Hawaii and whose rising branch over the subtropical western North Pacific as seen in Fig. 11a. For the ENSO/PDO composite (Fig. 12b), a cyclonic moisture flux circulation again prevails over the midlatitude ocean and moisture flux convergence anomalies remain to be found over the eastern North Pacific. Moreover, the region indicating moisture divergence is quite extensive, covering the Hawaiian Islands and the eastern portion of the western North Pacific. Again, this feature corresponds well with Fig. 11b in which deep and broad descending motions are noticed from 150°W to 150°E over the subtropical ocean.

7. Summary

A long-term Hawaii rainfall index (HRI) is constructed using records from 27 stations since 1905. On the interannual time scale, Hawaii tends to be dry during most of the El Niño and wet during most of the La Niña events. After applying a low-pass filter, the HRI exhibits a clear signal of interdecadal variations since
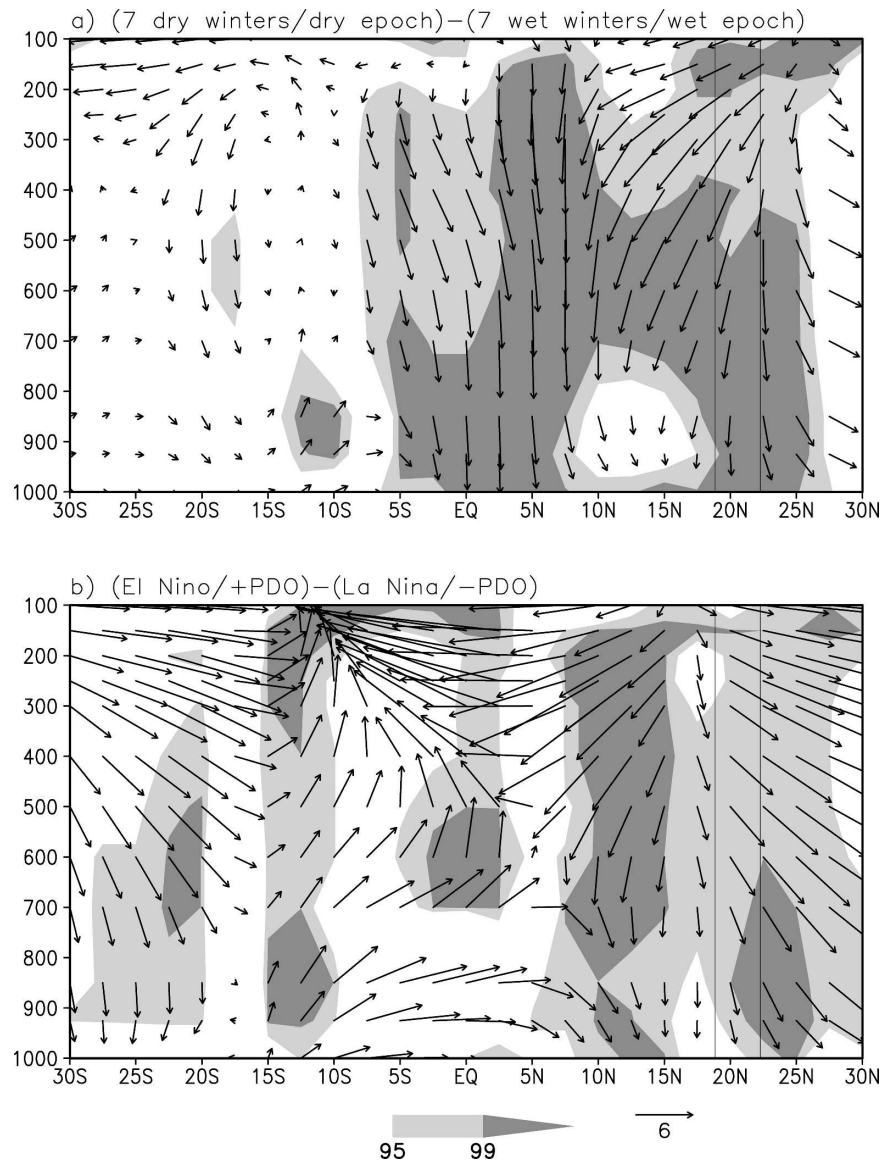
FIG. 10. Winter composites of north–south vertical circulation: (a) DRY minus WET and (b) (El Niño/+PDO) minus (La Niña/−PDO). Latitude–height section of meridional wind and negative pressure vertical velocity $(V, -\omega)$ is averaged over 165°–150°W. Shading is nonparametric Mann–Whitney test based on the vertical velocity. Light shading denotes 90% confidence level and dark shading for 95% confidence level of the vertical velocity difference. Unit vector in the horizontal direction is 6 m s^{-1} while that in the vertical direction is 0.03 Pa s^{-1}. The Hawaiian Islands are bordered approximately by two vertical lines.

1950. The HRI is negatively correlated with the Pacific decadal oscillation (PDO) index, with the correlation coefficients being significant at the 95% confidence level. A further analysis is performed to reveal spatial patterns of interannual and interdecadal winter rainfall variations for all 272 rainfall stations. Seven extremely dry and wet winters are selected from the dry and wet epochs, respectively. For simplicity, the composite of seven extremely dry winters during the dry epoch is

referred to as DRY, and the composite of seven extremely wet winters during the wet epoch is referred to as WET. These patterns are discussed relative to the joint El Niño–Southern Oscillation (ENSO) and PDO phases; that is, the composite difference between (El Niño/+PDO) and (La Niña/−PDO). Compared to the difference in ENSO/PDO phases, the magnitude of dry anomalies during the DRY minus WET winters tends to be enhanced.
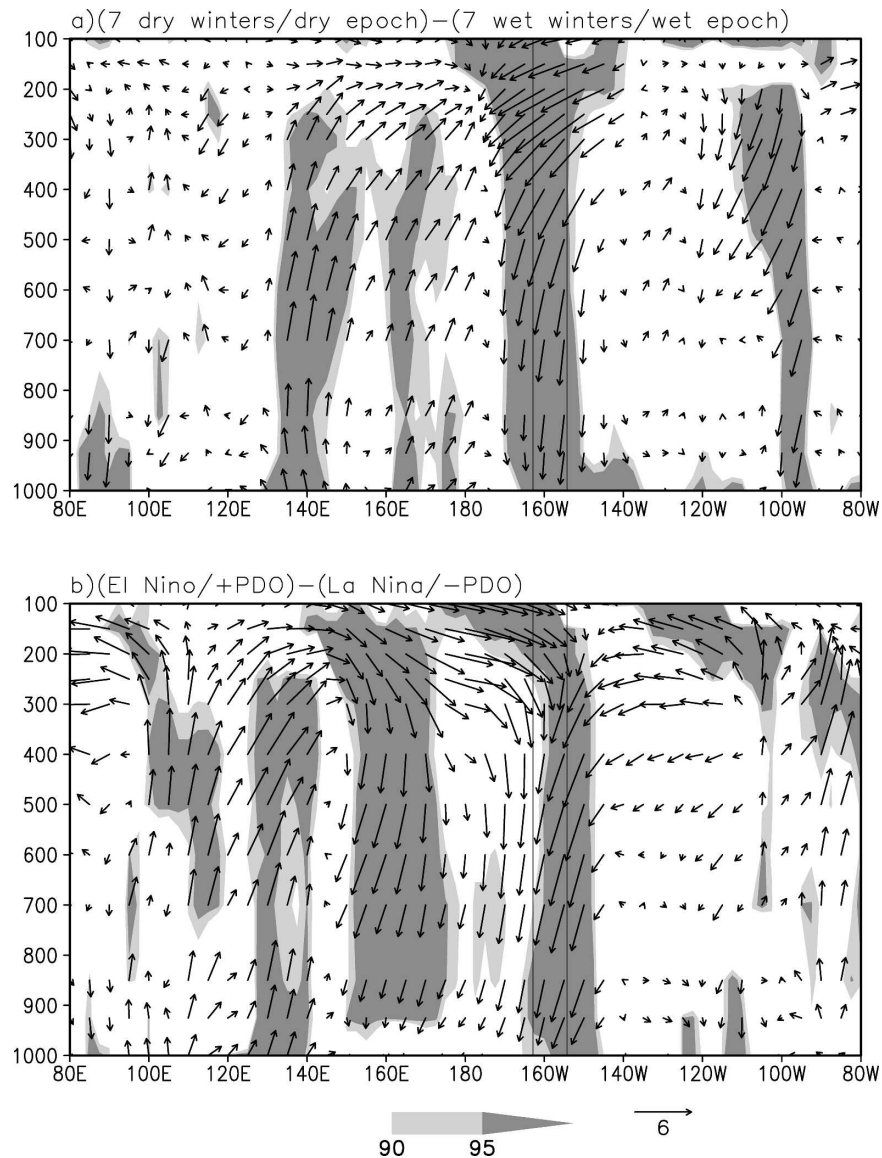
FIG. 11. Winter composites of east–west vertical circulation composites: (a) DRY minus WET, and (b) (El Niño/+PDO) minus (La Niña/−PDO). Longitude–height section of zonal wind and negative pressure vertical velocity (U, $-\omega$) is averaged over 15°–25°N. Shading is nonparametric Mann–Whitney test based on the vertical velocity. Light shading denotes 90% confidence level and dark shading for 95% confidence level of the vertical velocity difference. Unit vector in the horizontal direction is 6 m s^{-1}, while that in the vertical direction is 0.03 Pa s^{-1}. The Hawaiian Islands are bordered approximately by two vertical lines.

The atmospheric circulation composites associated with the above two extreme climatic stages are then investigated to reveal the physical causes. Results indicate similar patterns of the two climate stages. For example, common features include the deepening of the Aleutian low with a band of anomalous surface westerlies observed immediately to the north of Hawaii, a pool of cool water over the central North Pacific, and warm waters in the eastern North Pacific. The westerly

anomalies play an important role in reducing the trade wind strength over Hawaii, thus reducing the trade wind rainfall. For the height–latitude section, anomalously strong subsidence is noted over the Hawaii sector associated with the DRY minus WET samples, and this descending motion is deeper and stronger than that when the La Niña/−PDO is subtracted from the El Niño/+PDO batches. The height–longitude section during the DRY minus WET winters features an
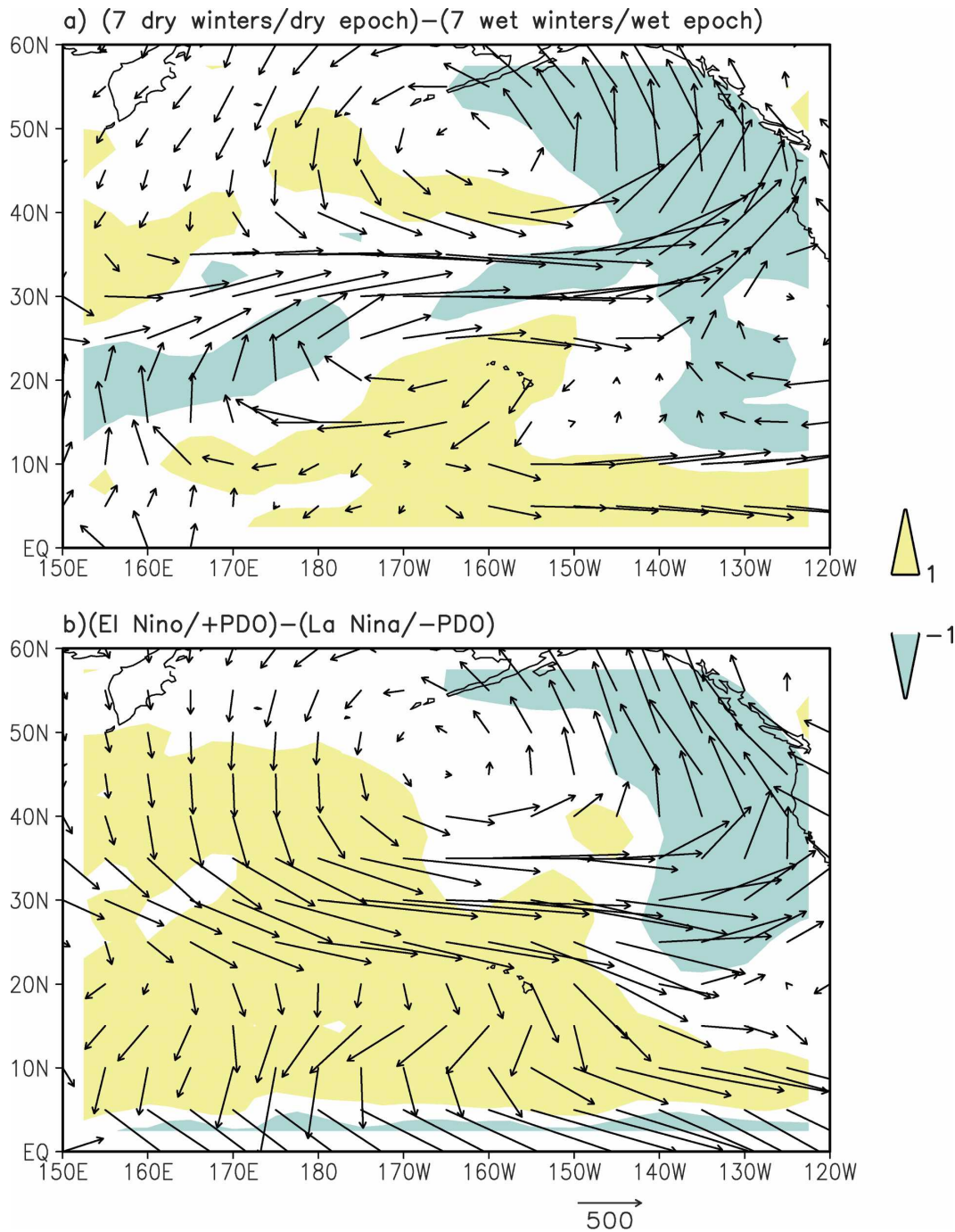
FIG. 12. Winter composites of vertically integrated moisture flux (qu, qv) (vectors) and moisture flux divergence $D(Q)$ (shading): (a) DRY minus WET, and (b) (El Niño/+PDO) minus (La Niña/−PDO). Values for $D(Q)$ greater than 1 mm day^{-1} are in yellow, and values less than −1 mm day^{-1} are in blue. The unit for flux is g (cm s)$^{-1}$.

anomalous regional east–west circulation cell over the subtropical North Pacific with a pronounced sinking branch over Hawaii. The sinking motion observed from both the zonal and meridional cross sections hinders the development of subtropical cyclones, upper-level

lows, and the passage of midlatitude frontal systems to the Hawaiian Islands. These features, together with the reduced easterly trade winds, possibly result in low winter rainfall for the islands. The vertically integrated moisture flux reveals anomalous divergence patterns

over the Hawaiian Islands, providing unfavorable conditions for convection to occur during the DRY minus WET winters.

REFERENCES

Barnston, A. G., M. Chelliah, and S. B. Goldenberg, 1997: Documentation of a highly ENSO-related SST region in the equatorial Pacific. *Atmos.–Ocean,* **35,** 367–383.

Blumenstock, H. L., and S. Price, 1967: Climates of the United States—Hawaii. U.S. Dept. of Commerce, ESSA, Climatography of the United States 60-51, 27 pp.

Bove, M. C., 2000: PDO modification of U.S. ENSO climate impacts. M.S. thesis, Dept. of Meteorology, The Florida State University, 103 pp.

Cayan, D. R., and D. H. Peterson, 1989: The influence of North Pacific atmospheric circulation on streamflow in the west. *Aspects of Climatic Variability in the Pacific and the Western Americas*, D. H. Peterson, Ed., *Geophys. Monogr.,* No. 55, Amer. Geophys. Union, 375–397.

Chen, Y.-L., and J. Feng, 1995: The influences of inversion height on precipitation and airflow over the Island of Hawaii. *Mon. Wea. Rev.,* **123,** 1660–1676.

Chu, P.-S., 1989: Hawaiian drought and Southern Oscillation. *Int. J. Climatol.,* **9,** 619–631.

——, 1995: Hawaii rainfall anomalies and El Niño. *J. Climate,* **8,** 1697–1703.

——, 2002: Large-scale circulation features associated with decadal variations of tropical cyclone activity over the central North Pacific. *J. Climate,* **15,** 2678–2689.

——, A. J. Nash, and F. Porter, 1993: Diagnostic studies of two contrasting rainfall episodes in Hawaii: Dry 1981 and wet 1982. *J. Climate,* **6,** 1457–1462.

Clark, J. D., and P.-S. Chu, 2002: Interannual variation of tropical cyclone activity over the central North Pacific. *J. Meteor. Soc. Japan,* **80,** 403–418.

Garbrecht, J. D., and F. E. Rossel, 2002: Decadal-scale precipitation increase in the Great Plains at the end of the 20th century. *J. Hydrol. Eng.,* **7,** 64–75.

Gershunov, A., 1998: ENSO influence on intraseasonal extreme rainfall and temperature frequencies in the contiguous United States: Implications for long-range predictability. *J. Climate,* **11,** 3192–3203.

——, and T. P. Barnett, 1998: Interdecadal modulation of ENSO teleconnections. *Bull. Amer. Meteor. Soc.,* **79,** 2715–2725.

——, and D. R. Cayan, 1999: North Pacific interdecadal oscillation seen as factor in ENSO-related North American climate anomalies. *Eos, Trans. Amer. Geophys. Union,* **80,** 25–30.

Lau, K.-M., and H. Weng, 1995: Climate signal detection using wavelet transform: How to make a time series sing. *Bull. Amer. Meteor. Soc.,* **76,** 2391–2402.

Lyons, S. W., 1982: Empirical orthogonal function analysis of Hawaiian rainfall. *J. Appl. Meteor.,* **21,** 1713–1729.

Mantua, N. J., S. R. Hare, Y. Zhang, J. M. Wallace, and R. C. Francis, 1997: A Pacific interdecadal climate oscillation with impacts on salmon production. *Bull. Amer. Meteor. Soc.,* **78,** 1069–1079.

Meisner, B. N., 1976: A study of Hawaiian and Line Islands rainfall. UHMET-76-04, Dept. of Meteorology, University of Hawaii, 83 pp.

Minobe, S., 1997: An oscillation of period 50–70 years over the North Pacific. *Geophys. Res. Lett.,* **24,** 683–686.

——, and N. Mantua, 1999: Interdecadal modulation of interannual atmospheric and oceanic variability over the North Pacific. *Progress in Oceanography,* Vol. 43, Pergamon, 163–192.

Morrison, I., and S. Businger, 2001: Synoptic structure and evolution of a Kona low. *Wea. Forecasting,* **16,** 81–98.

Newell, R. E., J. W. Kidson, D. J. Vincent, and G. J. Boer, 1974: *The General Circulation of the Tropical Atmosphere*. MIT Press, 370 pp.

Newman, M., G. P. Compo, and M. A. Alexander, 2003: ENSO-forced variability of the Pacific decadal oscillation. *J. Climate,* **16,** 3853–3857.

Quenouille, M. A., 1952: *Associated Measurements*. Butterworths, 242 pp.

Ramage, C. S., 1962: The subtropical cyclone. *J. Geophys. Res.,* **67,** 1401–1411.

Rasmusson, E. M., and T. H. Carpenter, 1982: Variations in tropical sea surface temperature and surface wind fields associated with the Southern Oscillation/El Niño. *Mon. Wea. Rev.,* **110,** 354–384.

Ropelewski, C. F., and M. S. Halpert, 1987: Global and regional scale precipitation patterns associated with the El Niño/Southern Oscillation. *Mon. Wea. Rev.,* **115,** 1606–1626.

Taylor, G. E., 1984: Hawaiian winter rainfall and its relation to the Southern Oscillation. *Mon. Wea. Rev.,* **112,** 1613–1619.

Torrence, C., and G. P. Compo, 1998: A practical guide to wavelet analysis. *Bull. Amer. Meteor. Soc.,* **79,** 61–78.

Trenberth, K. E., 1997: The definition of El Niño. *Bull. Amer. Meteor. Soc.,* **78,** 2771–2777.

——, and J. W. Hurrell, 1994: Decadal atmosphere-ocean variations in the Pacific. *Climate Dyn.,* **9,** 303–319.

Walker, G. T., and E. W. Bliss, 1932: World weather V. *Mem. Roy. Meteor. Soc.,* **4,** 119–139.

Weng, H., and K.-M. Lau, 1994: Wavelet, period doubling, and time-frequency localization with application to organization of convection over the tropical western Pacific. *J. Atmos. Sci.,* **51,** 2523–2541.

Wilks, D. S., 1995: *Statistical Methods in the Atmospheric Sciences*. Academic Press, 467 pp.

Zhang, Y., J. M. Wallace, and D. S. Battisti, 1997: ENSO-like interdecadal variability: 1900–93. *J. Climate,* **10,** 1004–1020.